10-1-2006

A continuum model on the nanomesa and nanowell formation in Langmuir-Blodgett ferroelectric polymeric films

Jiang Yu Li
University of Washington, USA

Yang Luo
University of Nebraska - Lincoln

Mengjun Bai
University of Nebraska-Lincoln, baime@missouri.edu

Stephen Ducharme
University of Nebraska, sducharme1@unl.edu

Published in *Journal of the Mechanics and Physics of Solids* **54**:10, (October 2006), pp. 2162-2182;
doi:10.1016/j.jmps.2006.03.008 http://www.sciencedirect.com/science/journal/00225096

Submitted September 30, 2005; revised January 4, 2006; accepted March 28, 2006;
published online June 9, 2006.

A continuum model on the nanomesa and nanowell formation in Langmuir–Blodgett ferroelectric polymeric films

JiangYu Li[a,*], Yang Luo[b], Mengjun Bai[c, d], and Stephen Ducharme[c]

[a] Department of Mechanical Engineering, University of Washington, USA
[b] Department of Engineering Mechanics, University of Nebraska–Lincoln, USA
[c] Department of Physics and Astronomy and Center for Materials Research and Analysis, University of Nebraska–Lincoln, USA
[d] Present address: Department of Physics and Astronomy, University of Missouri-Columbia, Columbia, MO 65217, USA.
* Corresponding author. Tel.: +1 206 543 6226; fax: +1 206 685 8047.

Abstract
Spontaneous crystalline nanomesa and nanowell formation has recently been discovered in polyvinylidene fluoride trifluoroethylene [P(VDF–TrFE)] copolymer films developed by Langmuir–Blodgett (LB) deposition. In this paper, we propose a continuum field model to analyze this remarkable phenomenon, consisting of kinematics, energetics, and kinetics of pattern formation and evolution in P(VDF–TrFE) films. Linear perturbation analysis has been carried out to analyze the stability and growth of patterns under small perturbations, and finite difference numerical simulations have been implemented to simulate the morphologies and evolutions of nanomesas and nanowells. The effects of film thickness and a number of other material parameters have been considered in our simulations, which agree well with experimental observations. We expect that our modeling and simulation methods can be used to guide the design and optimization of nanomesa and nanowell patterns for technological applications.

Keywords: Self-organizing, Pattern formation, Nanomesa, Nanowell, Ferroelectric polymer

1. Introduction

Polyvinylidene fluoride (PVDF) is a non-conjugated fluorinated hydrocarbon polymer with a simple linear sequence of molecular structure $–(CH_2–CF_2)_n–$ (Lovinger, 1983 and Tashiro, 1995). The all-trans TTTT conformation is one of the basic forms of PVDF polymer chains, and the alternating trans-gauche TGT$\overline{G}$ conformation is also common, with G/$\overline{G}$ denoting ± 60° rotation of the dihedral bond. Additional ordered conformations in PVDF include the helical conformation TGTG and longer repeating sequence TTTG. These polymer chains usually are organized in crystalline lattices, among them the paraelectric α phase, in which the dipole moments of the alternating trans-gauche conformation cancel each other out, and ferroelectric β phase, where the dipole moments of the all-trans conformation lead to macroscopic polarization. To control the phase transition temperature of β phase, random copolymer of PVDF and trifluoroethylene (TrFE) has been developed (Tashiro, 1995).

A remarkable phenomenon of spontaneous crystalline nanomesa and nanowell formation has recently been discovered in P(VDF–TrFE) copolymer films developed by Langmuir–Blodgett (LB) deposition. After annealing an initially uniform one monolayer (ML) film at 125 °C for 1 h, an array of predominately disc-shaped nanomesas isolated from each other on the substrate appears, with average diameter 95 ± 22 nm and average thickness 8.7 ± 0.4 nm (Bai and Ducharme, 2004); see Figure 1 for the atomic force microscopy (AFM) image. The nanomesas are ferroelectric, with the same crystalline orientation and nearly the same transition temperature found in a continuous film (Bai and Ducharme, 2004 and Bune et al., 1998). As the number of the monolayers increases, more nanomesas develop, some joined into extended shapes, and tending toward percolation as the number of nanomesas increases. The 4-ML films are mostly filled in, resulting in a complementary pattern of nanowells with diameter 128 ± 37 nm and thickness 9.8 ± 3.3 nm. At 8-ML and thicker, the films remain continuous without nanowells, even after lengthy annealing at similar condition. This progression from sparse, isolated nanomesas, through extended shapes, to nanowells is evident in the AFM images of Figure 1.

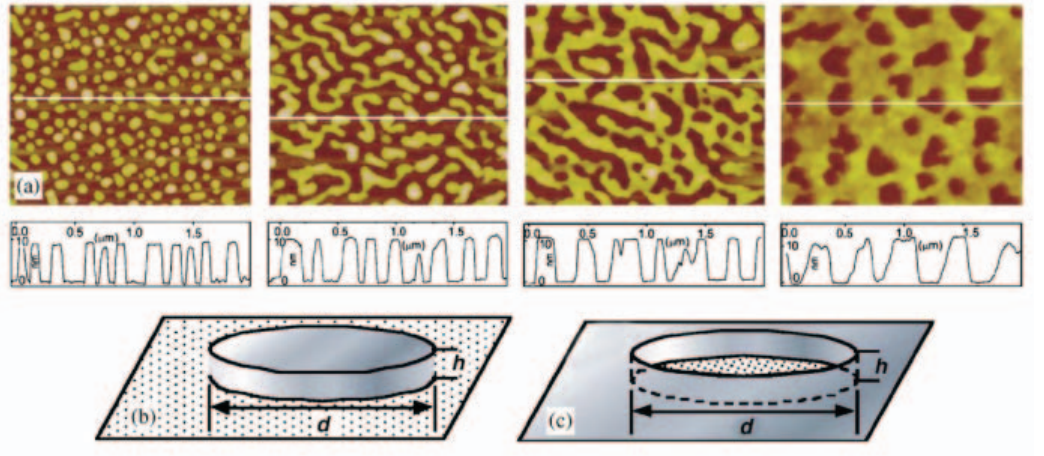

Figure 1. Images of nanomesa and nanowell obtained by annealing uniform thin films of thickness, L–R, 1, 2, 3, and 4 ML. Below each image is a height profile recorded along the white line in the image. (a) Room temperature AFM images, and associated height profiles from P(VDF–TrFE) copolymer LB films; (b and c) schematic illustration of nanomesa and nanowell.

Given the ferroelectricity and piezoelectricity of P(VDF–TrFE) LB films, the nanomesas are attractive for a number of applications including high-density non-volatile random-access memories, acoustic transducer arrays, and infrared imaging arrays. The nanomesa and nanowell patterns may also provide useful templates for the self-assembly of novel ferroelectric nanostructures. With the increasing demand for miniaturization of devices, enhancement of functionality, and increased storage density of energy and data (Zhang et al., 1998, Zhang et al., 2002, Li and Rao, 2004 and Li et al., 2004), fabrication of such functional nanostructures becomes increasingly important. However, for their technological potential to be fully realized, it is essential to understand the mechanism and process of nanomesa and nanowell formation to enable the tailoring of nanomesas and nanowells for the design and optimization of novel materials, structures, and devices.

In addition to the technological implications, such self-organizing and self-patterning phenomena are also important and appealing scientifically. They often occur in materials over many length scales by competing atomic or molecular interactions that might be difficult to detect otherwise (Muthukumar et al., 1997), and have been observed in many different material systems with rich thermodynamics, kinetics, and morphologies (Seul and Chen, 1993, Proville, 2002, Yang et al., 2004 and Lin and Granick, 2005). As a result, it is of fundamental and technological importance to understand the mechanism and process of nanomesa and nanowell formation in P(VDF–TrFE) films. This understanding may also shed light on self-organizing and self-patterning processes in other material systems at various length scales.

In this paper, we describe our theoretical analysis and numerical simulations on the formation of nanomesas and nanowells in P(VDF-TrFE) copolymer films. The preliminary results were reported in a recent letter (Li et al., 2005), and here we present the model development and numerical implementation in detail. It is not our intention to address the underlying molecular mechanism of nanomesa formation. Instead, we will focus on the modeling and simulation of the phenomena at the continuum level to guide the design and optimization of nanomesa and nanowell patterns. With the feature size of nanomesas and nanowells of the order of 100 nm, our continuum treatment is not only appropriate, but also much more efficient than molecular modeling. The approach we adopt here falls into the broad category of phase field theory (Chen, 2002), which has been applied by many to study pattern formations and evolutions in martensites (Artemev et al., 2001), ferroelectrics (Nambu and Sagala, 1994, Hu and Chen, 1997, Li et al., 2001 and Wang et al., 2004; Zhang and Bhattacharya, 2005a and Zhang and Bhattacharya, 2005b), magnetostrictive crystals (Shu et al., 2004), and binary epilayers (Suo and Lu, 2000 and Lu and Suo, 2001).

This paper is organized as follows. In Section 2, a continuum field model will be described, which consists of kinematics, energetics, and kinetics of pattern formation and evolution of P(VDF–TrFE) films. Linear perturbation analysis will then be carried out in Section 3 to analyze the stability and growth of patterns due to small perturbation of uniform films. Numerical implementation of the model will be presented in Section 4, where the evolution equation will be normalized and discretized, and fast Fourier transform (FFT) technique and semi-implicit scheme will be employed to speed up computations. Finally, the simulation results will be presented in Section 5 and compared with experimental observations, and the effects of various experimental parameters will be analyzed.

2. A continuum field model

Before going into mathematical details, we discuss our main ideas here. First of all, we note that regardless of the initial thickness of the uniform P(VDF–TrFE) films, the final thickness of nanomesas or nanowells is very consistent, approximately 9 nm. This suggests that the films prefer a certain thickness, which can be factored into the energetics. Indeed, it is well known that lamellar polymer crystals possess preferred thickness due to chain folding energetics (Sadler, 1987, Yamamoto, 1997 and Welch and Muthukumar, 2001), which was shown to be thermodynamically stable by Monte Carlo simulation (Doye and Frenkel, 1998). Secondly, for neighboring film segments with different thickness, it is reasonable to assume that there is an energy penalty due to the appearance of an interface, which implies that the film prefers a uniform thickness. This interfacial energy will drive the coarsening process when a pattern appears. The third point is more subtle. The polymer films will have a surface energy that depends on their chain morphology, or macroscopically, depends on the strain in the film. This strain-dependence leads to a surface stress that is also dependent on the film thickness. When the thickness of the film is not uniform, the surface stress becomes non-uniform, which will induce an elastic field in the film and substrate. This elastic field will drive the refining process when the pattern appears. As such, the feature size of the pattern will be determined by the competition between interfacial interactions and surface stress induced elastic interactions. This is the essence of our model. Note that we do not consider the dipolar interactions, because various experiments show that nanomesas and nanowells only form when the uniform P(VDF–TrFE) films are annealed in paraelectric phase above phase transition temperature (Bai and Ducharme, 2006). Next, we will present the main components of the model: kinematics, energetics, and kinetics.

2.1. Kinematics

We describe the state of P(VDF–TrFE) film by its surface concentration C, the number of monomer per unit surface area, when the polymeric film is a few nanometers thick. It is related to the volume concentration of P(VDF–TrFE) P, the number of monomers per unit volume by

$$C = Ph, \tag{1}$$

where h is the film thickness. During the formation of nanomesas and nanowells, the molecules of P(VDF–TrFE) relocate on the surface of the substrate, as described by the molecule relocation vector $\mathbf{I}$, such that $I_\alpha n_\alpha$ gives the number of molecules across a curve of unit length with $\mathbf{n}$ as normal, where the Greek subscripts range from 1 to 2 and repeated Greek subscripts are summed from 1 to 2, representing the two-dimensional coordinate of the film surface. As a result, the change in the concentration due to the material flow is

$$\delta C = -\delta I_{\alpha,\alpha}, \tag{2}$$

where the subscript comma is used to denote differentiation. The flow of the molecules is then given by the molecule flux vector $\mathbf{J}$, where $J_\alpha n_\alpha$ gives the number of molecules across a curve of unit length with $\mathbf{n}$ as normal per unit time. As such we have

$$\frac{\partial C}{\partial t} = -J_{\alpha,\alpha}. \tag{3}$$

As we will show later, the formation of nanomesas and nanowells from uniform P(VDF–TrFE) films is coupled with the elastic deformation of film and substrate, as described by the infinitesimal strain tensor ε,

$$\varepsilon_{ij} = \tfrac{1}{2}(u_{i,j} + u_{j,i}), \tag{4}$$

where **u** is the displacement vector of the film with respect to the fictitious unstressed state that has identical surface concentration as the patterned film, and the Latin subscripts range from 1 to 3 and repeated Latin subscripts are summed over 1–3. This elastic deformation is a response to the inhomogeneous distribution of surface stress $\gamma_{\alpha\beta}$, which is assumed to depend on the surface concentration of P(VDF–TrFE),

$$\gamma_{\alpha\beta} = \gamma\delta_{\alpha\beta}C, \tag{5}$$

where γ is the surface stress coefficient and $\delta_{\alpha\beta}$ is Kronecker delta. Note that the form of Equation (5) implies that the polymer film is isotropic, consistent with the circular shape of the nanomesas observed (Bai and Ducharme, 2004). This surface stress describes the dependence of film's surface energy on its strain, as we discuss in the next subsection.

2.2. Energetics

We propose that the formation of nanomesas and nanowells reduces the free energy of the system consisting of the film and substrate. The contributions to the energy include a surface term residing in P(VDF–TrFE) film and a bulk term residing in the film and substrate,

$$G = \int \Pi \,\mathrm{d}A + \int W \,\mathrm{d}V, \tag{6}$$

where Π is the surface energy density integrated over the surface area of the film, and W is the elastic energy density integrated over the volume of the film and substrate. It is clear that we adopt a continuum point of view here, which allows us to carry out modeling and simulation at large length scales relevant to materials and structures. We emphasize that the surface energy density Π incorporates all relevant molecular interactions in P(VDF–TrFE) films. In particular, we assume that it takes the following form:

$$\Pi = \alpha C_{,\beta}C_{,\beta} + g(C) + \gamma_{\alpha\beta}(C)\varepsilon_{\alpha\beta}, \tag{7}$$

where the first term penalizes the gradient of surface concentration C of P(VDF–TrFE) monomer, and thus leads to an interface energy when the surface concentration is non-uniform. The second term in (7) is the internal energy density per unit surface area, which we assume is a function of film thickness h, as we discussed earlier. Microscopically, this assumption implies that the internal energy density of a P(VDF–TrFE) nanomesa depends on its chain morphology. A similar assumption has been made for thin nematic films experiencing spinodal dewetting (Vandenbrouck et al., 1999), and we expect it will hold for LB films with thickness of a few nanometers. In particular, we assume that the internal energy density $g(C)$ is given by

$$g(C) = ah_r^2\left[\frac{C}{Ph_r} - 1\right]^2 C^2, \tag{8}$$

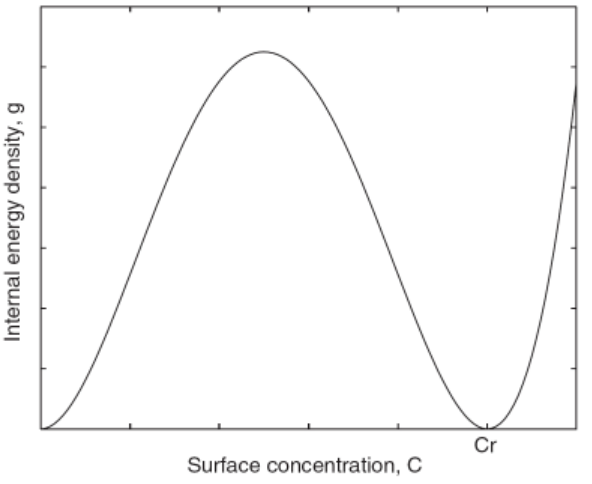

Figure 2. The internal energy per unit surface area of P(VDF–TrFE) films.

which possesses two minima thicknesses of 0 and h_r, as shown in Figure 2. The third term in (7) is a surface energy due to the strain of the film, with the coefficient $\gamma_{\alpha\beta}$ being the surface stress. On the surface of polymer film, we have

$$\sigma_{3\alpha} = \gamma_{\alpha\beta,\beta}, \quad \sigma_{33} = 0, \tag{9}$$

which results in a shear traction on the surface of the film when the surface stress is inhomogeneous. This shear traction will then lead to a strain field in the system, such that (Lu and Suo, 2001)

$$\varepsilon_{\alpha\alpha} = \frac{(v^2-1)\gamma}{\pi E} \int\int \frac{(x_1-\xi_1)(\partial C/\partial\xi_1) + (x_2-\xi_2)(\partial C/\partial\xi_2)}{[(x_1-\xi_1)^2 + (x_2-\xi_2)^2]^{3/2}} \, \mathrm{d}\xi_1 \, \mathrm{d}\xi_2, \tag{10}$$

where E is Young's modulus and v is Poisson's ratio of the film-substrate system. The elastic energy per unit volume, W, then takes the following quadratic form:

$$W = \frac{E}{2(1+v)} \left[\varepsilon_{ij}\varepsilon_{ij} + \frac{v}{1-2v} (\varepsilon_{kk})^2 \right]. \tag{11}$$

Note that this analysis requires a perfect bonding between the film and substrate, while in reality it is necessary for materials to flow to form the nanomesa and nanowell patterns. There is no inconsistency though, since the strain here is derived from displacement field that is measured with respect to the fictitious, patterned, yet unstressed film that has identical surface concentration distribution as the stressed and patterned film. In other words, the displacement due to the materials flow is excluded from the consideration, the deformation field due to the non-uniform surface stress is small, and thus the assumption of perfect bonding during the surface stress induced deformation is not unreasonable.

The elastic energy in the volume of the system can be determined from the stress and displacement at the surface of the film using divergence theorem, resulting in

$$\int W \, \mathrm{d}V = \frac{1}{2} \int \sigma_{3\alpha} u_\alpha \, \mathrm{d}A, \tag{12}$$

where it is assumed that the bottom surface of the system is traction free. In a similar fashion, we derive the surface energy due to the surface stress as

$$\int \gamma_{\alpha\beta}\varepsilon_{\alpha\beta}\,\mathrm{d}A = \int \gamma_{\alpha\beta}u_{\alpha,\beta}\,\mathrm{d}A = \int [(\gamma_{\alpha\beta}u_\alpha)_{,\beta} - (\gamma_{\alpha\beta,\beta}u_\alpha)]\,\mathrm{d}A. \tag{13}$$

The divergence theorem transforms the first term in the bracket to an integral over the boundary of the film, which disappears under the periodic boundary condition. Consequently, the bulk elastic energy and the surface energy are combined, resulting in

$$\int W\,\mathrm{d}V + \int \gamma_{\alpha\beta}\varepsilon_{\alpha\beta}\,\mathrm{d}A = -\frac{1}{2}\int \sigma_{3\alpha}u_\alpha\,\mathrm{d}A, \tag{14}$$

which is negative definite. In other words, the elastic deformation resulted from the surface stress leads to the reduction of free energy.

Combining all the terms together, we have the free energy of the system given as

$$G = \int \left[\alpha C_{,\alpha}C_{,\alpha} + g(C) - \frac{1}{2}\sigma_{3\alpha}u_\alpha\right]\mathrm{d}A. \tag{15}$$

It is clear now that the second term, the stored energy density $g(C)$, has two minima and thus will lead to pattern separation. The first term, the interface energy, will drive the pattern coarsening to reduce the interface area, while the last term, the total of elastic energy and surface energy, will drive the pattern refining to maximize $C_{,\alpha}$. The spontaneous nanomesa and nanowell formation is a consequence of the competition among the three energetic terms, and the balance of interface energy and elastic and surface energy determines the feature size of nanomesas and nanowells. It is noted that we have not considered the interaction energy between dipoles, since it is observed in experiments that nanomesas and nanowells are formed only when the films are annealed above the phase transition temperature in paraelectric phase (Bai and Ducharme, 2006).

2.3. Kinetics

The process of nanomesa and nanowell formation is driven by the reduction of free energy, where the total energy variation is given by

$$\delta G = \int \delta W\,\mathrm{d}V + \int \delta\Gamma\,\mathrm{d}A. \tag{16}$$

The first integral can be transformed using the divergence theorem as

$$\int \delta W\,\mathrm{d}V = \int \sigma_{ij}n_j\delta u_i\,\mathrm{d}A - \int \sigma_{ij,j}\delta u_i\,\mathrm{d}V, \tag{17}$$

where **n** is the surface normal. The variation of surface energy can be treated in a similar manner, leading to

$$\begin{aligned}\int \delta\Gamma\,\mathrm{d}A = &\int \left[-\left(\frac{\partial g}{\partial C} - 2\alpha\nabla^2 C + \gamma\delta_{\beta\gamma}\varepsilon_{\beta\gamma}\right)\delta I_\alpha + 2\alpha_0 C_{,\alpha}\delta C + \gamma_{\alpha\beta}\delta u_\beta\right]m_\alpha\,\mathrm{d}L \\ &+ \int \left[\left(\frac{\partial g}{\partial C} - 2\alpha\nabla^2 C + \gamma\delta_{\beta\gamma}\varepsilon_{\beta\gamma}\right)_{,\alpha}\delta I_\alpha - \gamma_{\alpha\beta,\beta}\delta u_\alpha\right]\mathrm{d}A,\end{aligned} \tag{18}$$

where **m** is the tangent of the curve bounding the surface, and

$$\nabla^2 = \frac{\partial^2}{\partial x_1^2} + \frac{\partial^2}{\partial x_2^2}.$$

Under a periodic boundary condition, the line integral in the equation disappears, and the total energy variation is given by

$$\delta G = \int \left[\left(\frac{\partial g}{\partial C} - 2\alpha \nabla^2 C + \gamma \delta_{\beta\gamma} \varepsilon_{\beta\gamma} \right)_{,\alpha} \delta I_\alpha + (\sigma_{3\alpha} - \gamma_{\alpha\beta,\beta}) \delta u_\alpha + \sigma_{33} \delta u_3 \right] \mathrm{d}A - \int \sigma_{ij,j} \delta u_i \, \mathrm{d}V. \tag{19}$$

Since the elastic deformation does not dissipate energy, the variation of free energy with respect to the elastic displacement vanishes, leading to

$$\sigma_{ij,j} = 0$$

in the bulk and

$$\sigma_{3\alpha} = \gamma_{\alpha\beta,\beta}, \quad \sigma_{33} = 0$$

on the surface, which we have already used in the previous subsection. On the other hand, the variation of free energy with respect to the molecule relocation dissipates energy, from which the driving force **F** for the nanomesa and nanowell formation can be established as

$$\int F_\alpha \delta I_\alpha \, \mathrm{d}A = -\delta G, \tag{20}$$

which is determined to be

$$F_\alpha = -\left(\frac{\partial g}{\partial C} - 2\alpha \nabla^2 C + \gamma \delta_{\beta\gamma} \varepsilon_{\beta\gamma} \right)_{,\alpha}. \tag{21}$$

The molecule flux is assumed to be linearly dependent on the driving force through the molecule mobility M,

$$J_\alpha = M F_\alpha, \tag{22}$$

which leads to a diffusion type of equation that defines the evolution of the concentration field

$$\frac{\partial C}{\partial t} = M \nabla^2 \left(\frac{\partial g}{\partial C} - 2\alpha \nabla^2 C + \gamma \delta_{\alpha\beta} \varepsilon_{\alpha\beta} \right). \tag{23}$$

This is the evolution equation that leads to the formation of nanomesas and nanowells. Before we try to solve this equation, it is worthwhile to discuss the conditions under which such a pattern will emerge in the films using linear perturbation analysis.

3. Linear perturbation analysis

In order to demonstrate the conditions of nanomesa and nanowell formation, we carry out linear perturbation analysis in this section. A small perturbation in the surface concentration can be represented by a superposition of its sinusoidal components. Con-

sider one such component here given by

$$C(x_1, t) = C_0 + A(t) \sin kx_1, \tag{24}$$

where C_0 is the uniform surface concentration, and $A \ll C_0$ and k are the amplitude and the wave-number of the perturbation, respectively, with $k = 2\pi/\lambda$, where λ is the wave length of the perturbation.

3.1. Stability of small perturbation

In order to study whether such perturbation will lead to pattern evolution, we consider the difference of the free energy before and after the perturbation. Before the perturbation, the concentration field is uniform, the film/substrate is stress-free, and the only energy contribution to the system is $g(C_0)$. After the perturbation, the concentration is no longer uniform, resulting in an additional interface energy per unit area given by

$$\frac{1}{\lambda}\int_0^{\lambda} \alpha\left(\frac{\partial C}{\partial x_1}\right)^2 \mathrm{d}x_1 = \frac{1}{2}\alpha k^2 A^2, \tag{25}$$

which drives the pattern to coarsen. The contribution from the internal energy density $g(C)$ per unit area is given by

$$\frac{1}{\lambda}\int_0^{\lambda} g(C)\,\mathrm{d}x_1 = g(C_0) + \frac{1}{4}g_2 A^2, \tag{26}$$

where g_2 is the Taylor expansion coefficient of $g(C)$ around C_0,

$$g(C) = g_0 + g_1(C - C_0) + \tfrac{1}{2}g_2(C - C_0)^2$$

with

$$\begin{aligned}
g_0 &= g(C_0) = ah_r^2\left(\frac{C_0}{Ph_r} - 1\right)^2 C_0^2,\\
g_1 &= \left.\frac{\partial g(C)}{\partial C}\right|_{C_0} = 2ah_r^2 C_0\left(\frac{C_0}{Ph_r} - 1\right)\left(2\,\frac{C_0}{Ph_r} - 1\right),\\
g_2 &= \left.\frac{\partial^2 g(C)}{\partial C^2}\right|_{C_0} = 2ah_r^2\left[6\left(\frac{C_0}{Ph_r}\right)^2 - 6\,\frac{C_0}{Ph_r} + 1\right] = 2ah_r^2\left[6\left(\frac{h_0}{h_r}\right)^2 - 6\,\frac{h_0}{h_r} + 1\right],
\end{aligned} \tag{27}$$

where $C_0 = Ph_0$ has been used in the derivation. In addition, under such a non-uniform concentration field, an elastic field arises in the film/substrate, and the surface traction due to the surface stress is given by

$$\sigma_{31} = \gamma\,\frac{\partial C}{\partial x_1} = A\gamma k \cos kx_1, \quad \sigma_{32} = \sigma_{33} = 0,$$

which leads to a displacement u_1 on the surface (Suo and Lu, 2000)

$$u_1 = \frac{2(1 - \nu^2)}{E}\,A\gamma \cos kx. \tag{28}$$

As such, the energy contribution due to the surface stress per unit surface area is

$$-\frac{1}{\lambda}\int_0^{\lambda}\frac{\sigma_{31}u_1}{2}\,\mathrm{d}x_1 = -\frac{1}{2}\left(\frac{1-v^2}{E}\right)k\gamma^2A^2, \tag{29}$$

which drives the pattern refining. The net variation of free energy per unit area due to the perturbation, ΔG, is then derived as

$$\Delta G = \frac{A^2}{2}\left(\frac{1}{2}g_2 - \frac{1-v^2}{E}k\gamma^2 + k^2\alpha\right), \tag{30}$$

which can be normalized as

$$\frac{\Delta G}{\alpha A^2/2l^2} = \frac{\mu}{2} - \frac{2\pi l}{\lambda} + \left(\frac{2\pi l}{\lambda}\right)^2, \tag{31}$$

where

$$\mu = \frac{\alpha g_2}{\gamma^4}\left(\frac{E}{1-v^2}\right)^2, \tag{32}$$

and

$$l = \frac{E\alpha}{(1-v^2)\gamma^2}. \tag{33}$$

From (31), it is clear that $\Delta G = 0$ has one solution for λ/l at $\mu = 0.5$, no solution at $\mu > 0.5$, and two solutions at $\mu < 0.5$, as shown in Figure 3. This suggests the free energy of the system cannot be reduced by surface concentration perturbation when $\mu > 0.5$, so that the uniform surface concentration is stable. On the other hand, when $\mu < 0.5$,

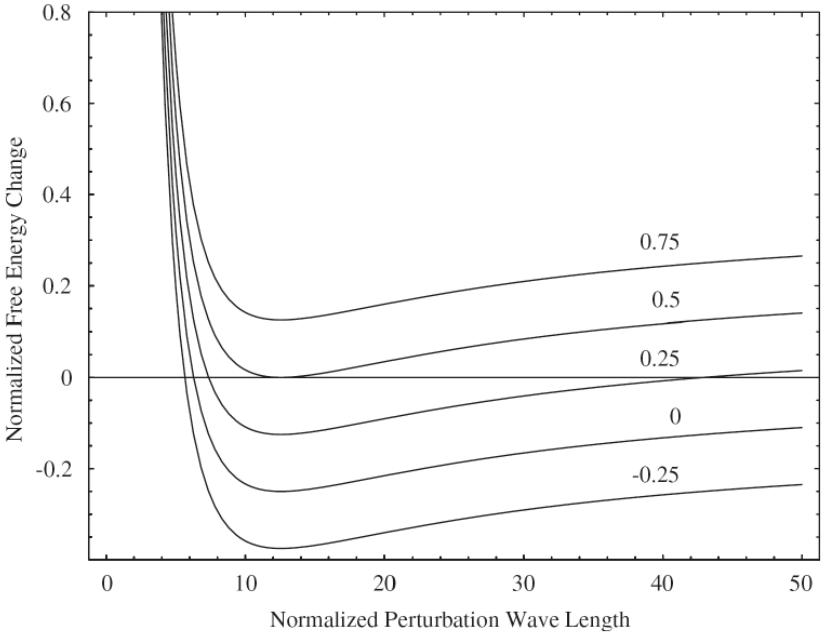

Figure 3. The change of normalized free energy ΔG as a function of the perturbation wave length λ/l at different μ.

the free energy can be reduced by a surface concentration perturbation of a certain wave length, indicating that the uniform surface concentration is unstable. The free energy is then minimized by $\lambda = 4\pi l$, suggesting an equilibrium feature size for nanomesas or nanowells. A similar change of stability has been observed in binary epilayers (Lu and Suo, 1999).

This stability analysis offers a number of predictions on the nanomesa and nanowell patterns that are consistent with experiments (Bai and Ducharme, 2004). First, it predicts that there is a critical parameter $\mu = 0.5$, above which the uniform surface concentration is stable against perturbation. This suggests that there is a critical initial thickness, above which the films will remain continuous and the nanomesa or nanowell will not form. Indeed, no nanomesas or nanowells are observed in P(VDF–TrFE) films of 8 ML and thicker. We also note that μ is proportional to α, the coefficient for interface energy, indicating that large interface energy will prevent the formation of nanomesas and nanowells. This is also supported by the experimental observation that nanomesas and nanowells only form when annealed in the paraelectric phase and are not observed when annealed in the ferroelectric phase. While the mobility of ferroelectric phase may play a role here (Bai and Ducharme, 2006), it may also be due to the depolarization field induced by the discontinuity of polarization at the interface if nanomesas or nanowells form in a ferroelectric P(VDF–TrFE), resulting in much higher interface energy, and thus prevents the formation of nanomesas or nanowells in ferroelectric P(VDF–TrFE). Second, it predicts that the feature size scales with $4\pi l$, which is proportional to the elastic constant $E/(1\text{-}\nu^2)$ of the film-substrate and inversely proportional to γ^2, with γ being the surface stress coefficient of the film. This is confirmed by experimental observation (Bai and Ducharme, 2006) that nanomesa size on an aluminum-coated silicon substrate is smaller than that on a non-coated silicon substrate. Aluminum does have smaller stiffness than silicon, although interface interactions and substrate roughness may also play a role. As the temperature increases, it is reasonable to assume that the surface stress in the film will be partially relieved, suggesting larger nanomesa size; this is also consistent with experimental observation (Bai and Ducharme, 2006). In addition, the feature size is independent of the initial thickness of the film in our model, while in experiments, it is observed that with the increase of the film's initial thickness, the smallest length scale in the nanomesa and nanowell patterns remains roughly the same, around 100–140 nm, even though the morphology varies.

3.2. Growth of small perturbation

We then consider the dynamic characteristics of one-dimensional perturbation growth along x_1 direction, with the evolution equation given by

$$\frac{\partial C}{\partial t} = M\left(g_2 \frac{\partial^2 C}{\partial x_1^2} - 2\alpha \frac{\partial^4 C}{\partial x_1^4} + \gamma \frac{\partial^3 u_1}{\partial x_1^3}\right). \tag{34}$$

For perturbation given by Equation (24), we obtain

$$\frac{\partial A(t)}{\partial t} = M\left[-g_2 A(t)k^2 - 2\alpha A(t)k^4 + \frac{2(1-\nu^2)}{E} A(t)\gamma^2 k^3\right], \tag{35}$$

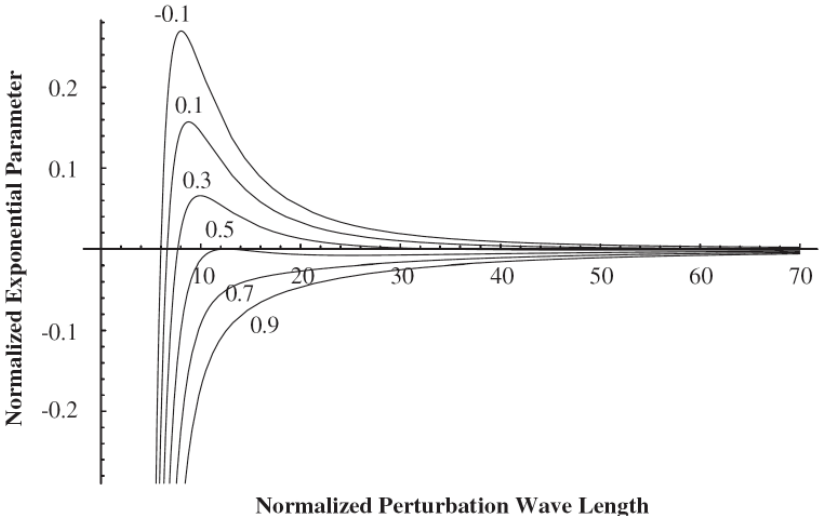

Figure 4. The normalized exponential parameter η as a function of the perturbation wave length λ / l at different μ.

which can be rewritten as

$$\frac{\mathrm{d}A(t)}{\mathrm{d}t} = \eta A(t) \tag{36}$$

with

$$\eta = M\left[-g_2 k^2 - 2\alpha k^4 + \frac{2(1-v^2)}{E}\gamma^2 k^3\right]. \tag{37}$$

The magnitude of perturbation is then solved as

$$A(t) = A(0)\exp(\eta t). \tag{38}$$

Clearly, the growth of perturbation is governed by the parameter η. When $\eta < 0$, the perturbation will decay so that the uniform concentration field is stable. On the other hand, when $\eta > 0$, the perturbation will grow so that the uniform concentration is not stable against small perturbation. In addition, larger η will lead to faster growth rate. In order to study the influence of perturbation wave length on the growth of perturbation, we further derive η as a function of wave length λ,

$$\frac{\eta}{2M\alpha/l^4} = -\left(\frac{2\pi l}{\lambda}\right)^2\left[\frac{\mu}{2} - \frac{2\pi l}{\lambda} + \left(\frac{2\pi l}{\lambda}\right)^2\right], \tag{39}$$

which is shown in Figure 4. From this figure, we can determine the exponential parameter η from the wave length λ so that the growth of perturbation can be analyzed. In particular, we have $\eta < 0$ whenever $\mu > 0.5$, suggesting that the perturbation will not grow. This agrees with the stability analysis in the previous subsection. We also note that smaller μ leads to larger η, and thus larger growth rate, which is also confirmed by our numerical simulations, as shown later. While we would like to make comparison with experimental observations, such dynamic characterization is very difficult and has not been carried out yet. Finally, we point out that the dynamic char-

acteristics reported here is also similar to those observations in the binary epilayers (Lu and Suo, 1999).

4. Numerical implementation

4.1. Normalization

In order to carry out the numerical simulation of nanomesa and nanowell formation, the evolution equation has to be normalized. We first note that there are two distinct lengths in the system. One is given by

$$b = \left(\frac{\alpha}{ah_r^2}\right)^{1/2}, \tag{40}$$

which scales with the distance over which the concentration field changes from the level of mesa to that of well. It can be regarded as the width of the pattern boundary. The other is l which we have already introduced in the previous section, and it results from the competition between pattern coarsening and refining. It defines the feature size of the nanomesa and nanowell patterns, as we discussed earlier. The ratio of these two length scales then defines a dimensionless parameter Q,

$$Q = \frac{b}{l} = \frac{(1-\nu^2)\gamma^2}{E(ah_r^2\alpha)^{1/2}}. \tag{41}$$

From the evolution equation, we also note that the diffusivity D scales with Mah_r^2/γ, and thus a diffusion time scale is introduced,

$$\tau = \frac{b^2}{D} = \frac{\alpha}{(ah_r^2)^2 M},$$

which resolves events occurring over the length scale of the pattern boundary width b.

We then normalize the surface concentration C in terms of the reference concentration C_r,

$$c = \frac{C}{C_r} = \frac{h}{h_r}, \tag{42}$$

normalize length with respect to b, and normalize time with respect to τ, which results in

$$\frac{\partial c}{\partial t} = \nabla^2\left\{ Y(c) - 2\nabla^2 c - \frac{Q}{\pi}\int\int \frac{(x_1-\xi_1)(\partial c/\partial\xi_1) + (x_2-\xi_2)(\partial c/\partial\xi_2)}{[(x_1-\xi_1)^2+(x_2-\xi_2)^2]^{3/2}}\,\mathrm{d}\xi_1\,\mathrm{d}\xi_2\right\}, \tag{43}$$

where

$$Y(c) = 2c(c-1)(2c-1)$$

Neither x nor t is relabeled for simplicity.

4.2. Fourier transform and discretization

The Fourier transform of the normalized evolution equation leads to

$$\frac{\partial c^*}{\partial t} = -k^2 Y^* - 2(k^4 - k^3 Q)c^*, \tag{44}$$

where

$$c^*(k_1, k_2, t) = \int_{-\infty}^{+\infty} \int_{-\infty}^{+\infty} c(x_1, x_2, t) \mathrm{e}^{-2\pi i(k_1 x_1 + k_2 x_2)} \, \mathrm{d}x_1 \, \mathrm{d}x_2 \tag{45}$$

and

$$k = 2\pi \sqrt{k_1^2 + k_2^2}. \tag{46}$$

Similarly, $Y^*(k_1,k_2,t)$ is the Fourier transform of $Y(x_1,x_2,t)$.

The transformed evolution equation is then discretized. An $L \times L$ square lattice is considered in real space (x_1, x_2), which is divided into $N \times N$ grids with grid size of $\Delta = L/N$. The corresponding cell in Fourier space is $1/\Delta \times 1/\Delta$, which forms a $N \times N$ grids with the grid size of $1/L$. A discrete Fourier transform will be used to convert the values of c and Y at the grid points in real space to those of c^* and Y^* at the grid points in Fourier space through the FFT technique. On the temporal scale a semi-implicit scheme is adopted for discretization (Chen, 2002). For a given time t and a time step Δt, we denote

$$c_n^* = c^*(k_1, k_2, t), \quad Y_n^* = Y^*(k_1, k_2, t), \quad c_{n+1}^* = c^*(k_1, k_2, t + \Delta t),$$

and replace Y^* by Y_n^*, c^* by c_{n+1}^*, and $\partial c^*/\partial t$ by $(c_{n+1}^* - c_n^*)/\Delta t$ leading to

$$c_{n+1}^* = \frac{c_n^* - k^2 Y_n^* \Delta t}{1 + 2(k^4 - k^3 Q)\Delta t}. \tag{47}$$

5. Simulation results and discussions

The model was implemented in a Fortran code using the following numerical algorithm:

(1) Initialize the concentration field with random roughness, $c_1 = c_0(1 \pm \delta c)$, using the random number generator.
(2) Evaluate $Y(c_n)$ with given c_n.
(3) Transform c_n to c_n^* and Y_n to Y_n^* using FFT.
(4) Evaluate c_{n+1}^*.
(5) Transform c_{n+1}^* to c_{n+1} using the inverse FFT.
(6) Go to step 2 until a stable pattern emerges, or a desired time limit is reached.

Our simulation is carried out on a 256 × 256 cell, with $\Delta t = 0.4\tau$ and the time limit $t =$ 20,000 Δt. The initial random roughness δc is assumed to be less than 0.5%, and h_r is assumed to be 10 nm. In the following subsections, both the morphologies and evolutions of the patterns will be studied. It is pointed out that in the simulations, only the initial thickness of the thin films h_0 and the dimensionless parameter Q are used as input. While h_0 has a clear physical meaning, it is difficult to estimate Q for various

films that corresponds to the particular experimental conditions, due to the difficulty in estimating parameters a, γ, and α. Nevertheless, we noted that Q is completely determined by material constants, and thus does not change with the initial thickness of the films, making it possible to determine it by fitting with a particular initial thickness and use that to simulate films of other initial thickness.

5.1. Pattern morphologies

We first consider the morphologies of the nanomesas and nanowells at $t = 20{,}000$. In fact very little change has been observed in the morphologies after $t = 10{,}000$.

5.1.1. The effect of initial thickness

To analyze the effect of initial thickness, we set $Q = 0.71$, and consider h_0 to be 2, 4, 5.5, and 8.5 nm, corresponding approximately to the thickness of copolymer films of 1 ML, 2 ML, 3 ML, and 4 ML. The comparison of experiments and simulations is shown in Figure 5. Clearly, the morphologies and height profiles obtained from our numerical simulations agree with the experimental observations well, capturing the pattern transition from the isolated round mesas to isolated extended mesas, then to the interconnected mesas, and finally to the isolated wells, as the initial thickness increases. The feature sizes of nanomesa and nanowells also agree with experimental measurements. In addition, it is observed that when the initial thickness is 10 nm or larger, the concentration field is stable and no pattern emerges, also consistent with both experimental observations and linear perturbation analysis.

5.1.2. The effect of Q

We also set $Q = b/l$ to be 0.1, 0.4, and 0.8, and analyzed its effects on the mesa pattern ($h_0 = 3$ nm), interconnected pattern ($h_0 = 5$ nm), and well pattern ($h_0 = 7$ nm), as shown in Figure 6. It is clear that Q has little influence on the morphologies of patterns, but has significant influence on the feature sizes of patterns. Larger Q leads to smaller feature size, since it is defined as the ratio of b and l. The simplest way to control Q is probably through the stiffness of materials E, as stiffer material leads to smaller Q, and thus larger feature size. This is consistent with experimental observation that nanomesa size on an aluminum-coated silicon substrate is smaller than that on a non-coated silicon substrate. Q also scales with surface stress coefficient γ. As the temperature increases, it is reasonable to assume that the surface stress in the film will be partially relieved, leading to larger nanomesa size, which is also consistent with experimental observation (Bai and Ducharme, 2006).

Our simulations offer a number of predictions on nanomesa and nanowell patterns, with pattern morphology controlled by the initial thickness of film and feature size controlled by material characteristics through dimensionless parameter Q. As such we expect that it can be used to guide the design and manipulations of nanomesas and nanowells.

5.2. Evolutions and dynamics

We next consider the dynamics of nanomesa and nanowell evolution, with the morphologies at different time steps monitored. The dynamic characterization of pattern evolution is very difficult to carry out experimentally and is not currently available, and we expect that our simulations can offer great insight into the evolution dynamics of nanomesas and nanowells.

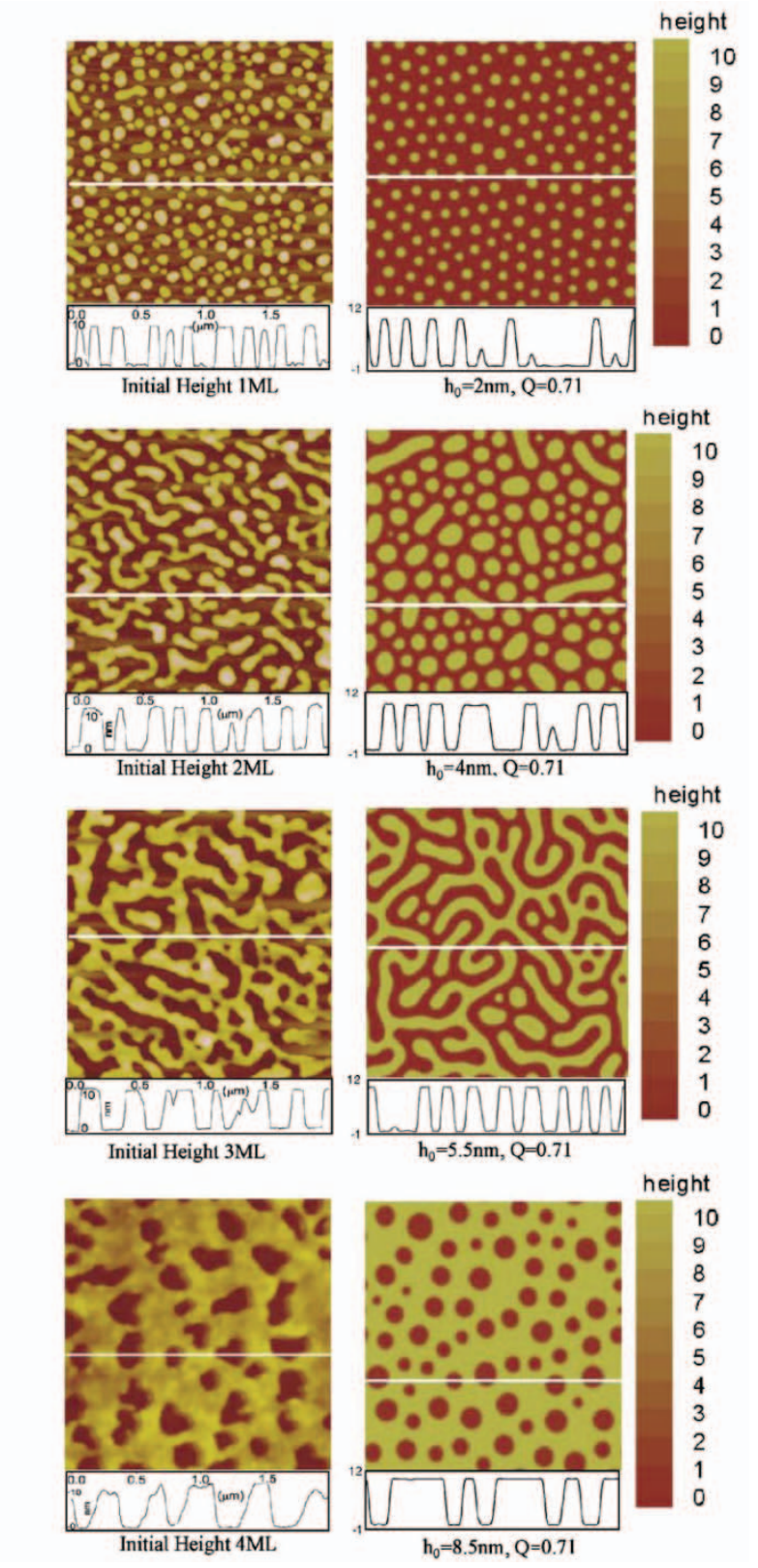

Figure 5. AFM images and height profiles (left column) and the corresponding simulations (right column) of P(VDF–TrFE) copolymer films of different initial thickness.

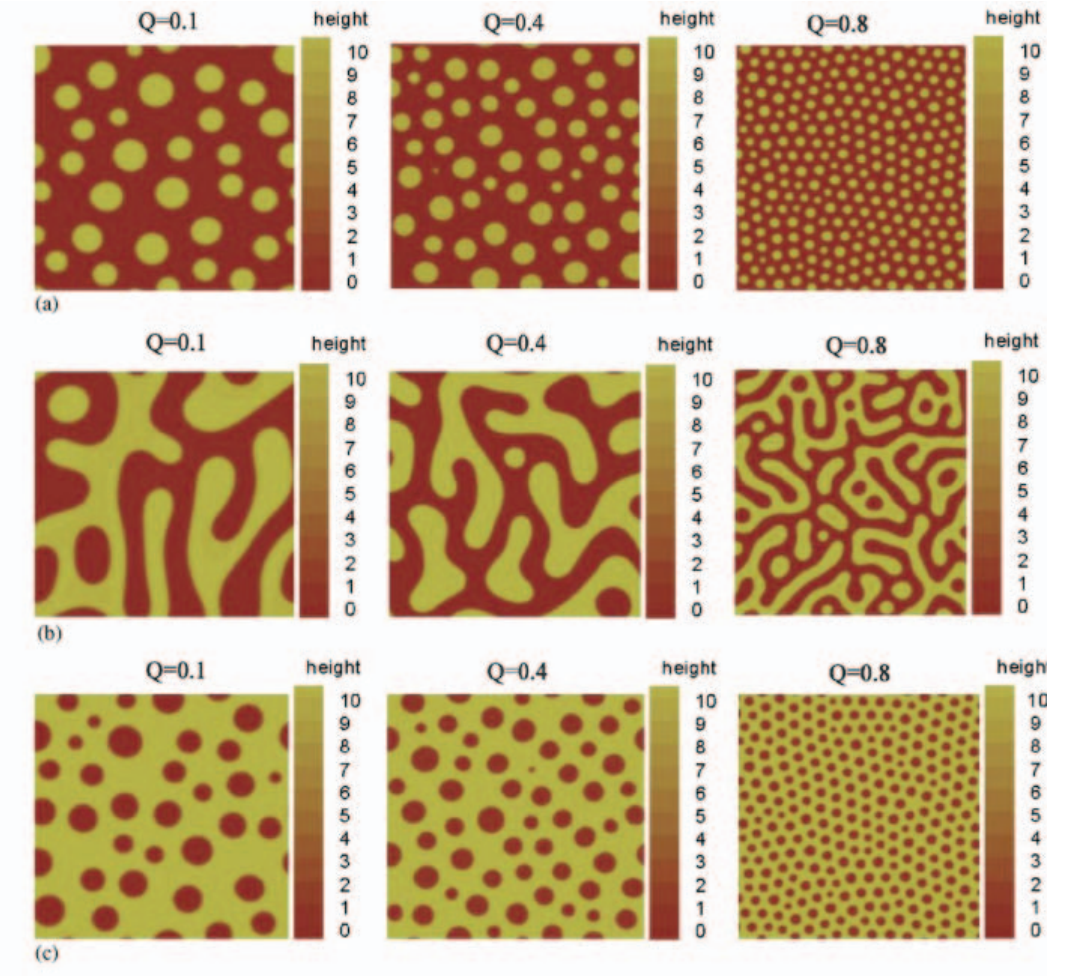

Figure 6. The comparison of simulated pattern morphologies and feature sizes under different Q and h_0. (a) $h_0 = 3$ nm, (b) $h_0 = 5$ nm and (c) $h_0 = 7$ nm.

5.2.1. The effect of initial thickness

We first consider the pattern evolution of copolymer films of different initial thickness, $h_0 = 3, 5, 7$ nm, with $Q = 0.6$, corresponding to a mesa pattern, an interconnected pattern, and a well pattern, respectively. The morphologies at $t = 50$, 500, 2000, 10 000 are shown in Figure 7. All three films exhibit the similar dynamic characteristics. Pattern separation occurs at $t < 50$, followed by the fast growth of pattern controlled by coarsening mechanism. The growth slows down considerably after $t > 1000$, and the pattern is slowly stabilized afterward. In addition, we note that the pattern in thicker films grow faster. For example, at $t = 50$, a clear pattern has emerged in films of 5 and 7 nm thickness, but not in film of 3 nm thickness. The patterns of 5 and

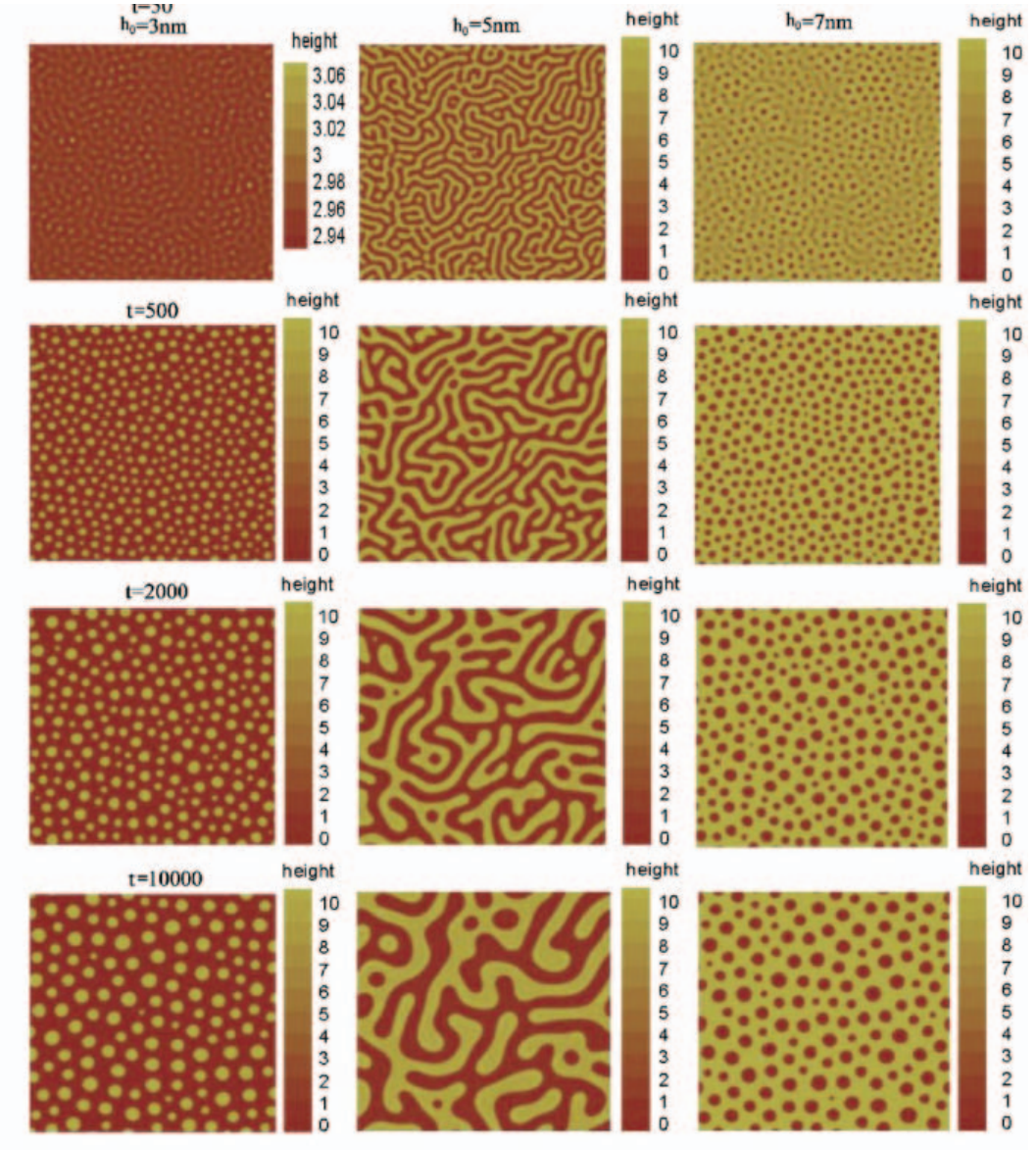

Figure 7. Comparison of simulated pattern evolution for different initial thickness with $Q = 0.6$.

7 nm films are stabilized by $t = 10{,}000$, while significant growth is observed for 3 nm film after $t = 10{,}000$. This is consistent with our linear stability analysis, where larger h_0 leads to smaller g_2, and thus larger η, which suggests a faster growth rate.

5.2.2. The effect of Q

We then consider the effect of Q on the evolution of nanomesas and nanowells, with the initial thickness set to be 4 nm and Q chosen to be 0.3 and 0.8. The patterns

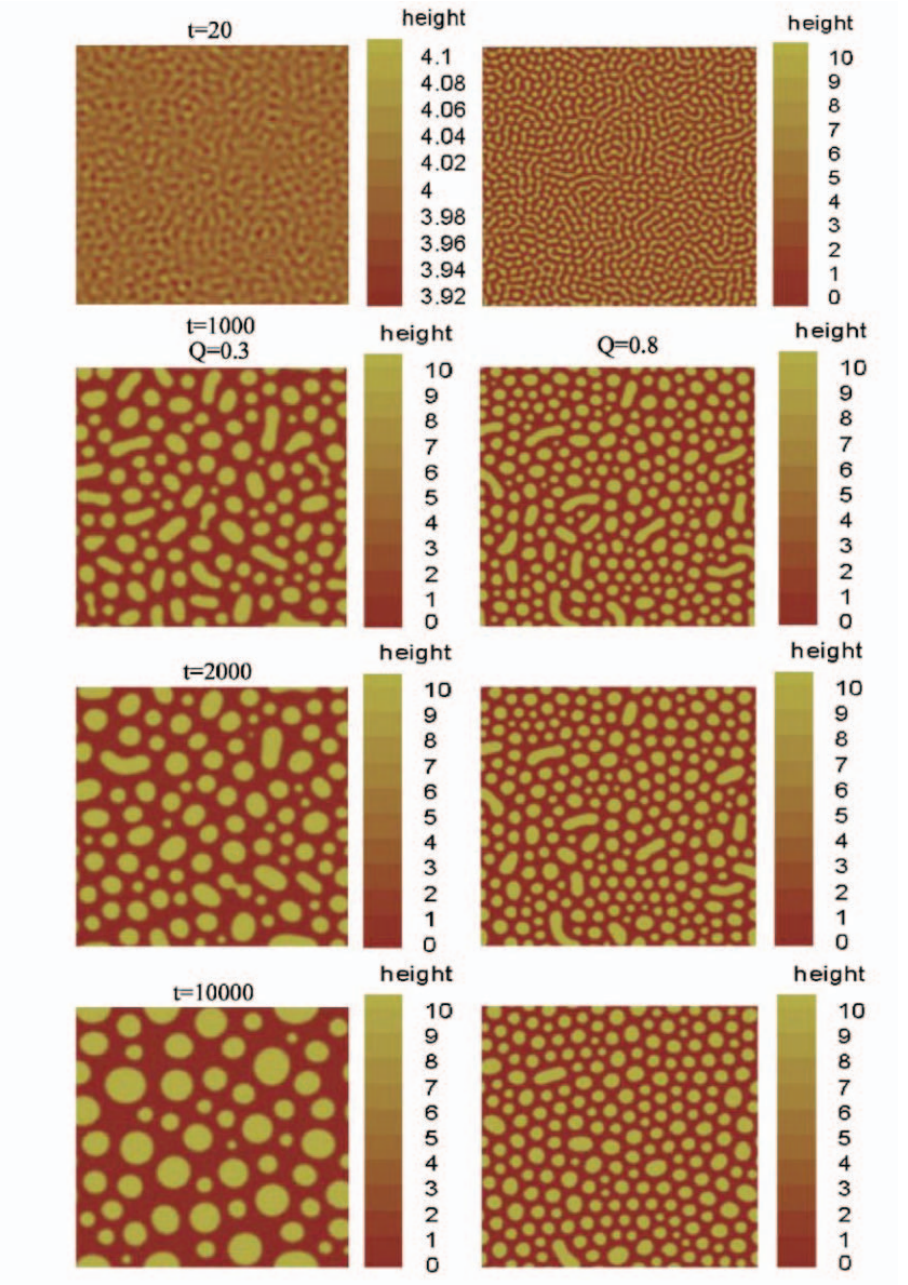

Figure 8. Comparison of simulated pattern evolution for different Q with the initial thickness $h_0 = 4$ nm; left column: $Q = 0.3$; right column: $Q = 0.8$.

at $t = 20$, 1,000, 2,000, 10,000 are shown in Figure 8, where it is observed that larger Q results in larger growth rate. For example, a clear pattern emerges in the film of $Q = 0.8$ at $t = 20$, earlier than the film of $Q = 0.3$. This is because the feature size in films of larger Q is smaller, leading to faster growth rate.

6. Concluding remarks

In summary, a continuum field model has been developed to analyze the formation of nanomesas and nanowells in P(VDF–TrFE) copolymer films of a few nanometer thickness. Linear perturbation analysis and numerical simulations have been carried out, which offers a number of predictions that are consistent with experimental observations. We expect that our modeling and simulation methods described here can be used to guide the design and optimization of nanomesa and nanowell patterns for technological applications.

Acknowledgments

We acknowledge the support of the National Science Foundation Nanomanufacturing Program (DMI-0300014) and the American Chemical Society Petroleum Research Fund Type G Grant (PRF# 39526-G5B).

References

ARTEMEV *ET AL.,* 2001 – A. Artemev, Y. Jin, and A.G. Khachaturyan, Three-dimensional phase field model of proper martensitic transformation, *Acta Materialia* **49** (2001), pp. 1165–1177.

BAI AND DUCHARME, 2004 – M. J. Bai and S. Ducharme, Ferroelectric nanomesa formation from polymer Langmuir–Blodgett films, *Appl. Phys. Lett.* **85** (2004), pp. 3528–3530.

BAI AND DUCHARME, 2006 – M. J. Bai and S. Ducharme, Effects of annealing conditions on ferroelectric nanomesa self-assembly. *J. Phys.: Condens. Matter.,* (2006), accepted.

BUNE *ET AL.,* 1998 – A. V. Bune, V. M. Fridkin, S. Ducharme, L. M. Blinov, S. P. Palto, A. V. Sorokin, S. G. Yudin, and A. Zlatkin, Two-dimensional ferroelectric films, *Nature* **391** (1998), pp. 874–877.

CHEN, 2002 – L. Q. Chen, Phase-field models for microstructure evolution, *Annu. Rev. Mater. Res.* **32** (2002), pp. 113–140.

DOYE AND FRENKEL, 1998 – J. P. K. Doye and D. Frenkel, Mechanism of thickness determination in polymer crystals, *Phys. Rev. Lett.* **81** (1998), pp. 2160–2163.

HU AND CHEN, 1997 – H. L. Hu and L. Q. Chen, Computer simulation of 90° ferroelectric domain formation in two-dimensions, *Mater. Sci. Eng. A* **238** (1997), pp. 182–191.

LI AND RAO, 2004 – J. Y. Li and N. Rao, Micromechanics of ferroelectric polymer-based electrostrictive composites, *J. Mech. Phys. Solids* **52** (2004), pp. 591–615.

LI *ET AL.,* 2001 – Y. L. Li, S. Y. Hu, Z. K. Liu, and L. Q. Chen, Phase-field model of domain structures in ferroelectric thin films, *Appl. Phys. Lett.* **78** (2001), pp. 3878–3880.

LI *ET AL.*, 2004 – J. Y. Li, C. Huang, and Q. M. Zhang, Enhanced electromechanical properties in all-polymer percolative composites, *Appl. Phys. Lett.* **84** (2004), pp. 3124–3126.

LI *ET AL.,* 2005 – J. Y. Li, Y. Luo, M. J. Bai, and S. Ducharme, Nanomesa and nanowell formation in Langmuir–Blodgett polyvinylidene fluoride trifluoroethylene copolymer films, *Appl. Phys. Lett.* **87** (2005), p. 213116.

LIN AND GRANICK, 2005 – Z. Q. Lin and S. Granick, Patterns formed by droplet evaporation from a restricted geometry, *J. Amer. Chem. Soc.* **127** (2005), pp. 2816–2817.

LOVINGER, 1983 – A. J. Lovinger, Ferroelectric polymers, *Science* **220** (1983), pp. 1115–1121.

LU AND SUO, 1999 – W. Lu and Z. Suo, Coarsening, refining, and pattern emergence in binary epilayers, *Z. Metallkd.* **99** (1999), pp. 956–960.

LU AND SUO, 2001 – W. Lu and Z. Suo, Dynamics of nanoscale pattern formation of an epitaxial monolayer, *J. Mech. Phys. Solids* **49** (2001), pp. 1937–1950.

MUTHUKUMAR *ET AL.,* 1997 – M. Muthukumar, C. K. Ober, and E. L. Thomas, Competing interactions and levels of ordering in self-organizing polymeric materials, *Science* **277** (1997), pp. 1225–1232.

NAMBU AND SAGALA, 1994 – S. Nambu and D. A. Sagala, Domain formation and elastic long-range interaction in ferroelectric perovskites, *Phys. Rev. B* **50** (1994), pp. 5838–5847.

PROVILLE, 2002 – L. Proville, Ordering of atomic monolayers on a (0 0 1) cubic crystal surface. *Phys. Rev. Lett.* **88** (2002), article number 046102.

SADLER, 1987 – D. M. Sadler, New explanation for chain folding in polymers, *Nature* **326** (1987), pp. 174–176.

SEUL AND CHEN, 1993 – M. Seul and V. S. Chen, Isotropic and aligned stripe phases in a monomolecular organic film, *Phys. Rev. Lett.* **70** (1993), pp. 1658–1661.

SHU *ET AL.,* 2004 – Y. C. Shu, M. P. Lin, and K. C. Wu, Micromagnetic modeling of magnetostrictive materials under intrinsic stress, *Mech. Mater.* **36** (2004), pp. 975–997.

SUO AND LU, 2000 – Z. Suo and W. Lu, Compositional modulation and nanophase separation in a binary epilayer, *J. Mech. Phys. Solids* **48** (2000), pp. 211–232.

TASHIRO, 1995 – K. Tashiro, Crystal structure and phase transition of PVDF and related copolymers. In: H. S. Nalwa, Editor, *Ferroelectric Polymers*, Marcel Dekker, New York (1995), pp. 63–181.

VANDENBROUCK *ET AL.,* 1999 – F. Vandenbrouck, M. P. Valignat, and A. M. Cazabat, Thin nematic films: metastability and spinodal dewetting, *Phys. Rev. Lett.* **82** (1999), pp. 2693–2696.

WANG *ET AL.,* 2004 – J. Wang, S. Q. Shi, L. Q. Chen, Y. L. Li, and T. Y. Zhang, Phase field simulations of ferroelectric/ferroelastic polarization switching, *Acta Materialia* **52** (2004), pp. 749–764.

WELCH AND MUTHUKUMAR, 2001 – P. Welch, M. Muthukumar, M. Molecular mechanisms of polymer crystallization from solution. *Phys. Rev. Lett.* **87** (2001), article number 218302.

YAMAMOTO, 1997 – T. Yamamoto, Molecular dynamics simulation of polymer crystallization through chain folding, *J. Chem. Phys.* **107** (1997), pp. 2653–2663.

YANG ET AL., 2004 – B. Yang, F. Liu, and M. G. Lagally, Local strain-mediated chemical potential control of quantum dot self-organization in heteroepitaxy. *Phys. Rev. Lett.* **92** (2004), article number 025502.

ZHANG AND BHATTACHARYA, 2005a – W. Zhang and K. Bhattacharya, A computational model of ferroelectric domains. Part I: model formulation and domain switching, *Acta Materialia* **53** (2005), pp. 185–198.

ZHANG AND BHATTACHARYA, 2005b – W. Zhang and K. Bhattacharya, A computational model of ferroelectric domains. Part II: grain boundaries and defect pinning, *Acta Materialia* **53** (2005), pp. 199–209.

ZHANG ET AL., 1998 – Q. M. Zhang, V. Bharti, and X. Zhao, Giant electrostriction and relaxor ferroelectric behavior in electro-irradiated poly(vinylidene fluoride-trifluoroethylene) copolymer, *Science* **280** (1998), pp. 2101–2104.

ZHANG *ET AL.,* 2002 – Q. M. Zhang, H. F. Li, M. Poh, F. Xia, Z. Y. Cheng, H. S. Xu, and C. Huang, An all-organic composite actuator material with a high dielectric constant, *Nature* **419** (2002), pp. 284–287.